Preprint typeset in JHEP style - HYPER VERSION

CERN Preprint No.xxxxxx
FNAL Preprint No.yyyyyy

Constraining couplings of top quarks to the Z boson in $t\bar{t} + Z$ production at the LHC

Raoul Röntsch

Fermilab, Batavia, IL 60510, USA
Email: rontsch@fnal.gov

Markus Schulze

PH Department, TH Unit, CERN, 1211 Geneva 23, Switzerland
Email: markus.schulze@cern.ch

Abstract: We study top quark pair production in association with a Z boson at the Large Hadron Collider (LHC) and investigate the prospects of measuring the couplings of top quarks to the Z boson. To this date these couplings have not been constrained in direct measurements and only the LHC will allow such a determination for the first time. Our calculation improves previous coupling studies through the inclusion of next-to-leading order (NLO) QCD corrections in production and decays of all unstable particles. We treat top quarks in the narrow-width approximation and retain all NLO spin correlations. To determine the sensitivity of a coupling measurement we perform a binned log-likelihood ratio test based on normalization and shape information of the angle between the leptons from the Z boson decay. The obtained limits include statistical uncertainties as well as leading theoretical systematics from residual scale dependence and parton distribution functions. We find that with 300 fb^{-1} of data at an energy of 13 TeV the vector and axial $t\bar{t}Z$-coupling can be constrained to $C_{\mathrm{V}} = 0.24^{+0.39}_{-0.39}$ and $C_{\mathrm{A}} = -0.60^{+0.14}_{-0.18}$, at the 95% confidence level. This is a reduction of uncertainties by 25% and 42%, respectively, compared to an analysis based on leading-order predictions. We also translate these results into limits on dimension-six operators contributing to the $t\bar{t}Z$-interactions beyond the Standard Model.

Contents

1. Introduction

After run I of the Large Hadron Collider (LHC) at $\sqrt{s} = 7$ and 8 TeV, we look back on a highly successful research program. Already this first phase of exploring a new energy regime has provided many exciting results: the Higgs boson was discovered [1, 2], its quantum numbers and couplings are highly constrained, and many Standard Model (SM) measurements are competitive with previous ones, if not exceeding them. Furthermore, a plethora of searches for signals of new physics have been undertaken, reaching out into the multi-TeV region as well as exploring small deviations of SM parameters. The absence of any spectacular signal of new physics highly constrains many minimal extensions of the SM and, at the same time, opens up new ways for experimental searches and theoretical model building. These developments represent a remarkably fast progress and demonstrate the potential of the LHC in the years to come.

One particularly promising class of SM processes is top quark pair production in association with gauge bosons or a Higgs boson. Due to their relatively high production threshold these processes were not accessible at the Tevatron. In contrast, the high energy and large luminosity of the upcoming LHC runs will produce sufficiently many events to allow detailed studies of these processes. Progress in this direction has already been made with cross section measurements of $t\bar{t}+\gamma$ production by ATLAS [3] at 7 TeV and CMS [4] at 8 TeV. First events for the processes $t\bar{t} + Z/W$ have also been reported in Refs. [5, 6]. It is exciting to envision future studies of these processes with direct measurements of the couplings and new sensitivity to physics beyond the Standard Model.

In this paper we focus on the determination of the top quark to Z boson couplings through $t\bar{t}Z$ production at the LHC. This process is a *direct* probe of the $t\bar{t}Z$ interactions which distinguishes it from other indirect probes such as the LEP measurements of the ρ-parameter [7] and the $Z \to b\bar{b}$ branching ratio [8]. The SM unambiguously predicts the strength of these couplings and it is known that higher order corrections modify the leading order values only minimally [9]. On the other hand, extensions of the SM which address e.g. dynamic electroweak symmetry breaking typically induce larger deviations. Popular examples are certain variants of Supersymmetry [10, 11] or Little Higgs Models [12, 13]. More generally, any new fermion which mixes with the third generation quarks might induce deviations to the $t\bar{t}Z$ SM couplings. Hence also 4th generation quarks [14, 15], top-color models [16] and extra-dimensional extensions of space-time [17] have to be considered. It is therefore important to know to what extent LHC experiments are sensitive to physics beyond the SM in $t\bar{t}Z$ production. Clearly, this is not only a question of experimental sensitivity but also depends crucially on our theoretical understanding of the production and decay dynamics of the $pp \to t\bar{t}Z$ process.

The ability of LHC experiments to constrain the $t\bar{t}Z$ couplings was first considered in a series of studies by Baur, Juste, Orr and Rainwater [18,19]. The authors identified suitable observables which are sensitive to vector and axial couplings as well as to the weak electric and magnetic dipole moments. The tri-lepton signature with semi-hadronically decaying top quarks and a leptonically decaying Z boson turns out to provide a good compromise between clean signature and large enough cross section. But even decay modes with a Z boson decaying into neutrinos yield additional sensitivity [19]. Their analyses show that sensitivity to the form factor of the vector current is relatively weak and limits can only be placed within a factor of three wrt. the SM value. In contrast, the form factor of the axial current can be pinned down to about 20% accuracy. The authors of Ref. [20] perform a similar analysis using the more modern language of effective operators. This allows them to relate $t\bar{b}W$ and $t\bar{t}Z$ couplings in a combined study of single top and $t\bar{t}Z$ production.

In the context of this work it is important to emphasize that all previous coupling studies were performed at leading-order and large residual scale uncertainty was identified [18] as the main obstacle to stronger constraints on the $t\bar{t}Z$ couplings. It is the aim of this paper to reduce these uncertainties through a NLO QCD calculation for $t\bar{t}Z$ production and decay into a realistic final state with leptons, jets and missing energy. The hadronic production of $t\bar{t}Z$, with stable top quarks and a stable Z boson, was previously calculated at NLO QCD accuracy by Lazopoulos, McElmurry, Melnikov, and Petriello [21], and by Kardos, Papadopoulos, and Trocsanyi [22]. The latter calculation was also interfaced to a parton shower [23], accounting for the decays of the top quarks and Z boson through the spin uncorrelated parton shower approximation. Further hadronization effects were studied in Ref. [24]. Since our coupling analysis relies on studying leptonic opening angles we believe that spin correlations are crucial for a correct interpretation of the results. We therefore account for NLO QCD spin correlations in the decay of top quarks and hadronically decaying W bosons. This includes the full one-loop corrections as well as soft, collinear and wide angle gluon emission off the top quark decay chain. Spin correlations of the leptonically decaying Z boson are included as well. While including all spin correla-

tions, we approximate top quarks and the Z boson as close to on-shell in the narrow-width approximation. This approximation is parametric in Γ/m and its wide range of validity in $t\bar{t}$ production has been studied in Refs. [25–28].

It is interesting to note that the $t\bar{t}Z$ couplings may also be directly probed through single top production in association with a Z boson. Indeed, the inclusive cross section of tZ plus its charge conjugate process $\bar{t}Z$ is comparable to the inclusive $t\bar{t}Z$ cross section and NLO QCD predictions are given in Ref. [29]. It turns out that this process is also the leading background to a $t\bar{t}Z$ signal while other backgrounds such as $pp \to WZb\bar{b}jj$ are almost negligible [18]. However, it is possible to separate $t\bar{t}Z$ and tZ production by cutting on forward jets and demanding a high jet multiplicity, including two b-tagged jets [29]. We will therefore consider only the $t\bar{t}Z$ process in this paper, and defer the study of the couplings using $tZ + \bar{t}Z$ (or a combination of both processes) to a later date.

Finally, let us note that a coupling analysis is not the only scenario in which the process $pp \to t\bar{t}Z$ is interesting. The semi-hadronic decay mode of the top quark pairs together with the leptonic Z decay is background to several tri-lepton and same-sign lepton searches with additional jets and missing energy. Those signatures can arise from gluino decays of Supersymmetry, in Universal Extra Dimensions as well as in models with fermionic top quark partners. Furthermore, the invisible decay $Z \to \nu\bar{\nu}$ produces a top pair plus a large amount of missing transverse energy, and is therefore an irreducible background to searches for scalar or fermionic top quark partners decaying into top quarks plus dark matter candidates. While we do not address these topics in this paper, it would be interesting to study the effects of NLO corrections when strong selection cuts are applied on this background.

2. Outline of the calculation

In this section, we briefly discuss the features of our calculation. We consider the tri-lepton signature $pp \to t\bar{t}+Z \to t(\to \ell\nu b)\,\bar{t}(\to jj\bar{b})\,Z(\to \ell\ell)$ which profits from a large cross section due to the hadronic decay of one W boson and the lepton multiplicities from the remaining W and Z bosons. In our results we will sum over all combination of $e^{\pm}$ and $\mu^{\pm}$ in the final state, allowing either t or $\bar{t}$ to decay leptonically. Application of the narrow-width approximation for top quarks and the Z boson allows us to separate production and decays stage according to

$$\mathrm{d}\sigma_{pp\to\ell\ell\ell\nu b\bar{b}jj} = \mathrm{d}\sigma_{pp\to t\bar{t}+Z}\;\mathrm{d}\mathcal{B}_{t\to b\ell\nu}\;\mathrm{d}\mathcal{B}_{\bar{t}\to\bar{b}jj}\;\mathrm{d}\mathcal{B}_{Z\to\ell\ell}\;+\;\mathcal{O}(\Gamma_t/m_t,\,\Gamma_Z/M_Z), \qquad (2.1)$$

where $\mathrm{d}\sigma$ denotes the production cross section and $\mathrm{d}\mathcal{B}_{X\to Y} = \mathrm{d}\Gamma_{X\to Y}/\Gamma_X^{\mathrm{tot}}$ are the partial branching fractions. The use of the narrow width approximation neglects contributions which are parametrically suppressed by $\mathcal{O}(\Gamma/m)$, arising from a largely off-shell top quark or Z boson. Severe selection cuts on final state particles can violate this approximation when distorting the Breit-Wiegner line shape of the resonance. In our analysis we aim for a large cross section and only place mild cuts required by experimental detector acceptance.

Hence, we believe the narrow-width is an excellent approximation for our study[1]. We also neglect the contribution from the decay $t \to Wb + Z$ since the available phase space for on-shell top quarks is tiny and $\mathcal{B}_{t\to WbZ} \approx 3 \times 10^{-6}$ [30–33].

2.1 NLO QCD correction

At leading order, the production of $t\bar{t}Z$ occurs through the gg and $q\bar{q}$ partonic channels. At next-to-leading order QCD, these channels receive real and virtual corrections, while real emission corrections open up the partonic channels qg and $\bar{q}g$. We also include NLO QCD corrections to the top quark decays and the hadronically decaying W boson; consequently their total widths are included at LO and NLO as well. Eq. (2.1) expanded up to NLO accuracy reads,

$$\begin{aligned}
\mathrm{d}\sigma^{\mathrm{NLO}}_{pp\to\ell\ell\ell\nu b\bar{b}jj} &= \mathrm{d}\sigma^{\mathrm{LO}}_{pp\to t\bar{t}Z}\,\mathrm{d}\mathcal{B}^{\mathrm{LO}}_{t\to b\ell\nu}\,\mathrm{d}\mathcal{B}^{\mathrm{LO}}_{\bar{t}\to\bar{b}jj}\,\mathrm{d}\mathcal{B}_{Z\to\ell\ell}\;(1+\chi) \\
&+ \mathrm{d}\sigma^{\delta\mathrm{NLO}}_{pp\to t\bar{t}Z+X}\,\mathrm{d}\mathcal{B}^{\mathrm{LO}}_{t\to b\ell\nu}\,\mathrm{d}\mathcal{B}^{\mathrm{LO}}_{\bar{t}\to\bar{b}jj}\,\mathrm{d}\mathcal{B}_{Z\to\ell\ell} \\
&+ \mathrm{d}\sigma^{\mathrm{LO}}_{pp\to t\bar{t}Z}\left(\mathrm{d}\mathcal{B}^{\delta\mathrm{NLO}}_{t\to b\ell\nu+X}\,\mathrm{d}\mathcal{B}^{\mathrm{LO}}_{\bar{t}\to\bar{b}jj} + \mathrm{d}\mathcal{B}^{\mathrm{LO}}_{t\to b\ell\nu}\,\mathrm{d}\mathcal{B}^{\delta\mathrm{NLO}}_{\bar{t}\to\bar{b}jj+X}\right)\mathrm{d}\mathcal{B}_{Z\to\ell\ell}.
\end{aligned} \tag{2.2}$$

The factor $\chi = -2\Gamma_t^{\mathrm{tot},\delta\mathrm{NLO}}/\Gamma_t^{\mathrm{tot,LO}} - 2\Gamma_W^{\mathrm{tot},\delta\mathrm{NLO}}/\Gamma_W^{\mathrm{tot,LO}}$ arises from the α_s expansion of the total widths in the denominator. The virtual corrections are evaluated using a numerical OPP realization [34] of D-dimensional generalized unitarity [35–37] (for a review, see Ref. [38]). We extended the framework of Ref. [39] to account for color neutral bosons which requires new tree level recursion relations as well as an extension of the OPP procedure as described in e.g. Ref. [40]. Soft and collinear singularities in the real emission corrections are regularized using the dipole subtractions scheme of Refs. [41, 42] supplemented with a cut-off parameter for the finite dipole phase space [43–46]. The virtual and real corrections to the top quark decay and hadronic W boson decay are implemented analytically. Soft and collinear singularities in the real emission decay phase space are regularized using subtractions dipoles given in Ref. [47]. We also would like to point out our utilization of parallel computing features. We implemented a version of the Vegas integration algorithm which allows parallelization [48] via the Message-Passing-Interface (MPI) [49]. The observed speed-up in run time scales almost linear with the number of CPU cores used. This allows us to obtain a full NLO QCD prediction for the total cross section within a few hours on a modern desktop computer with 8 cores.

We perform several checks to ensure the correctness of our calculation. The squared amplitudes for tree level and real emission corrections are checked against MadGraph v.2.49 [50]. The cancellation of poles in $D-4$ of dimensional regularization between the virtual corrections and integrated dipoles has been verified for several phase space points. We also checked the finite part of the virtual amplitudes against the automated program `GoSam` [51] for a few phase space points and find very good agreement. Our framework also allows to turn the Z boson into an on-shell photon which we used to cross check against

[1] If necessary we can improve our results by allowing off-shell top quarks, Z boson and photons at LO. Non-factorizable corrections at NLO QCD which are suppressed by $\alpha_s\,\Gamma/m$ have to be neglected in our framework.

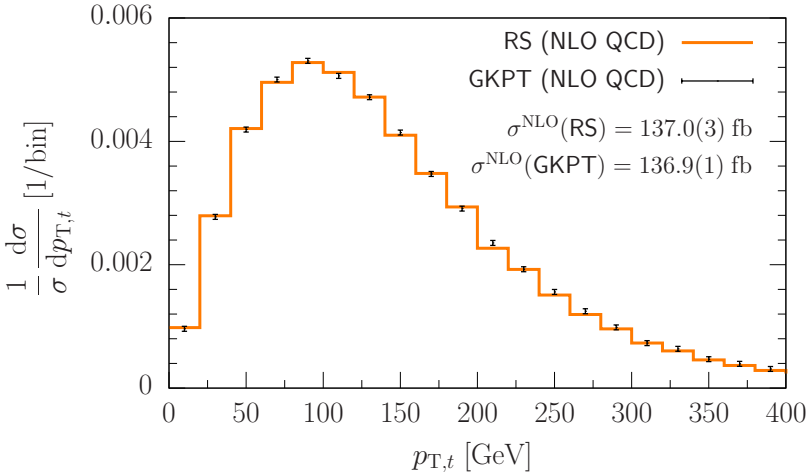

Figure 1: Shape comparison between our results (RS) and the ones of Ref. [24] (GKPT) for stable top quarks and Z boson. Shown is the normalized transverse momentum spectrum of the top quark at NLO QCD for the process $pp \to t\bar{t}Z$ at 7 TeV.

the amplitudes of Ref. [47]. At the level of the integrated cross section, we vary the cut-off parameter for the finite dipole phase space by at least one order of magnitude and verify independence on this parameter for the total cross section and kinematic distributions. The interface of production and decay amplitudes is checked by integrating over the full phase space and verifying the factorization into inclusive cross section for stable top quarks and Z boson times by their branching ratios, at NLO QCD. Finally, we compare our full hadronic results with a previous calculation [24] in the literature for stable top quarks and Z boson. The masses of the top quark, W boson and Z are $m_t = 173.5$ GeV, $M_W = 80.39$ GeV, and $M_Z = 91.187$ GeV. The electroweak coupling is defined through the Fermi constant $G_{\mathrm{F}} = 1.16639 \times 10^{-5}\,\mathrm{GeV}^{-2}$ and the weak mixing angle $\sin^2\theta_w = 1 - M_W^2/M_Z^2$. CTEQ6L1 [52] and CTEQ6.6M [53] parton distribution functions (pdfs) are used with $\alpha_s(M_Z) = 0.130$ and $\alpha_s(M_Z) = 0.118$, respectively. At the central factorization and renormalization scale of $\mu_0 = m_t + m_Z/2$, we find a leading order cross section of 103.5(1) fb and a next-to-leading order QCD cross section of 137.0(3) fb. This has to be compared with the results of Ref. [24] which are 103.5(1) fb and 136.9(1) fb, at leading and next-to-leading order QCD. The cross sections are in excellent agreement within the integration errors. Figure 1 also demonstrates good agreement in shape for the top quark p_{T} distribution between our results (RS) and Fig. 1a in Ref. [24] (GKPT).

2.2 $t\bar{t}Z$ couplings

The $t\bar{t}Z$ interaction Lagrangian in the SM can be written as

$$\mathcal{L}^{\mathrm{SM}}_{t\bar{t}Z} = \mathrm{i}e\,\bar{u}(p_t)\left[\gamma^\mu\left(C^{\mathrm{SM}}_{\mathrm{V}} + \gamma_5 C^{\mathrm{SM}}_{\mathrm{A}}\right)\right]v(p_{\bar{t}})Z_\mu, \tag{2.3}$$

with the electromagnetic coupling constant e. The vector and axial couplings are

$$\begin{aligned} C_{\mathrm{V}}^{\mathrm{SM}} =& \frac{T_t^3 - 2Q_t \sin^2\theta_w}{2\sin\theta_w \cos\theta_w}, \\ C_{\mathrm{A}}^{\mathrm{SM}} =& \frac{-T_t^3}{2\sin\theta_w \cos\theta_w}, \end{aligned} \tag{2.4}$$

where $Q_t = 2/3$ is the top quark electric charge, $T_t^3 = 1/2$ and θ_w is the weak mixing angle. New physics contributions to the $t\bar{t}Z$ couplings are most conveniently introduced by higher dimensional operators in the language of effective field theory. A minimal set of dimension-six operators for top quark production and decay have been categorized in Refs. [54–56]. In total there are 91 different operators which can be summarized into 20 different anomalous couplings, if on-shellness and gauge invariance is enforced [55]. For interactions of a Z boson with top quarks only four anomalous couplings, $C_{1/2,V/A}$, remain and Eq. (2.3) becomes

$$\mathcal{L}_{t\bar{t}Z} = \mathrm{i}e\bar{u}(p_t)\left[\gamma^\mu\big(C_{1,V} + \gamma_5 C_{1,A}\big) + \frac{\mathrm{i}\sigma_{\mu\nu}q_\nu}{M_Z}\big(C_{2,V} + \mathrm{i}\gamma_5 C_{2,A}\big)\right]v(p_{\bar{t}})Z_\mu, \tag{2.5}$$

with $\sigma_{\mu\nu} = \frac{\mathrm{i}}{2}[\gamma_\mu, \gamma_\nu]$ and $q_\nu = (p_t - p_{\bar{t}})_\nu$. The couplings can now be written in terms of the SM contribution plus deviations due to higher dimensional operators

$$\begin{aligned} C_{1,\mathrm{V}} &= C_{1,\mathrm{V}}^{\mathrm{SM}} + \left(\tfrac{v^2}{\Lambda^2}\right)\mathrm{Re}\left[C_{\phi q}^{(3,33)} - C_{\phi q}^{(1,33)} - C_{\phi u}^{33}\right], \\ C_{1,\mathrm{A}} &= C_{1,\mathrm{A}}^{\mathrm{SM}} + \left(\tfrac{v^2}{\Lambda^2}\right)\mathrm{Re}\left[C_{\phi q}^{(3,33)} - C_{\phi q}^{(1,33)} + C_{\phi u}^{33}\right], \end{aligned} \tag{2.6}$$

where

$$\begin{aligned} C_{\phi q}^{(3,33)} &= \mathrm{i}\left(\phi^\dagger \tau^a D_\mu \phi\right)\left(\bar{t}_{\mathrm{L}}\gamma^\mu \tau_a t_{\mathrm{L}}\right), \\ C_{\phi q}^{(1,33)} &= \mathrm{i}\left(\phi^\dagger D_\mu \phi\right)\left(\bar{t}_{\mathrm{L}}\gamma^\mu t_{\mathrm{L}}\right), \\ C_{\phi u}^{33} &= \mathrm{i}\left(\phi^\dagger D_\mu \phi\right)\left(\bar{t}_{\mathrm{R}}\gamma^\mu t_{\mathrm{R}}\right). \end{aligned} \tag{2.7}$$

For the exact definitions of fields in Eq. (2.7) we refer the reader to Ref. [55]. Clearly, $t_{\mathrm{R,L}}$ are the top quark spinors and ϕ is the SM Higgs doublet. In this work we will confine ourselves to the study of the above vector and axial couplings $C_{1,V/A}$. We therefore do not present the expansion of the $C_{2,V/A}$ couplings in terms of higher dimensional operators. These couplings correspond to the weak magnetic and electric dipole moments of the top quark. Their tree level value vanishes in the SM and $C_{2,V}$ receives one-loop corrections of $\mathcal{O}(10^{-4})$ [57]. The coupling $C_{2,A}$ receives finite contributions only beyond two-loops [58]. On the more technical side, the tensor structure that multiplies the $C_{2,V/A}$ couplings introduces the complication of non-renormalizable amplitudes at NLO QCD. While it is straightforward to handle such contributions our current implementation of the OPP integrand reduction method does not allow tensor ranks larger than N for N-point loop integrals. Such an extension of the OPP reduction algorithm has been outlined in the Appendix B of Ref. [59]. We will come back to this issue in a separate publication and

study the phenomenological implication of electroweak dipole moments in $t\bar{t}Z$ production.

We now would like to comment on existing constraints on the $t\bar{t}Z$ couplings. Clearly, those constraints are not obtained directly through on-shell production of a Z boson in association with top quark pairs. Instead, they arise from potential deviations which the higher dimensional operators in Eq. (2.6) introduce to the ρ parameter and the $Zb\bar{b}$ vertex in the SM. Those parameters are highly constrained through the experimental fits [60] of the ε parameters [61–63],

$$\varepsilon_1^{\text{exp}} = (5.6 \pm 1.0) \times 10^{-3}, \qquad \varepsilon_b^{\text{exp}} = (-5.8 \pm 1.3) \times 10^{-3}. \tag{2.8}$$

The SM predicts their values as $\varepsilon_1^{\text{SM}} = (5.21 \pm 0.08) \times 10^{-3}$ and $\varepsilon_b^{\text{SM}} = -(6.94 \pm 0.15) \times 10^{-3}$ [60]. The new physics contributions in Eq. (2.6) introduce the corrections [64]

$$\delta\varepsilon_1 = \frac{3m_t^2 G_{\text{F}}}{2\sqrt{2}\pi^2} \,\text{Re}\left[C_{\phi q}^{(3,33)} - C_{\phi q}^{(1,33)} + C_{\phi u}^{33} + \mathcal{O}\left(\frac{v^2}{\Lambda^2}\right)\right] \left(\frac{v^2}{\Lambda^2}\right) \log\left(\frac{\Lambda^2}{m_t^2}\right), \tag{2.9}$$

$$\delta\varepsilon_b = -\frac{m_t^2 G_{\text{F}}}{2\sqrt{2}\pi^2} \,\text{Re}\left[C_{\phi q}^{(3,33)} - C_{\phi q}^{(1,33)} + \frac{1}{4} C_{\phi u}^{33}\right] \left(\frac{v^2}{\Lambda^2}\right) \log\left(\frac{\Lambda^2}{m_t^2}\right). \tag{2.10}$$

The experimentally measured values in Eq. (2.8) can now be used to constrain the operators $C_{\phi q}^{(3,33)}$, $C_{\phi q}^{(1,33)}$ and $C_{\phi u}^{33}$. We will present the numerical results later in Sect. 3.4 together with our results from $t\bar{t}Z$ production. We also have to mention another experimental constraint. The measurements of the $Zb_{\text{L}}\bar{b}_{\text{L}}$ couplings from R_b and A_{FB}^b at LEP are in permille level agreement with the SM predictions [8]. This experimental fact together with the $\text{SU}(2)_{\text{L}}$ symmetry of the SM can be used to relate $C_{\phi q}^{(3,33)} \approx -C_{\phi q}^{(1,33)}$. Hence, one of these two operators can be eliminated from Eq. (2.6).

3. Results

3.1 NLO Results

In this section we describe the details of our numerical analysis and the results. We consider the process $pp \to t\bar{t} + Z \to t(\to \ell\nu b)\,\bar{t}(\to jj\bar{b})\,Z(\to \ell\ell)$ and sum over all combination of leptons $e^{\pm}, \mu^{\pm}$. We choose the following fixed input parameter

$$\begin{aligned} m_t &= 173 \text{ GeV}, & m_b &= 0 \text{ GeV}, \\ M_Z &= 91.1876 \text{ GeV}, & M_W &= 80.385 \text{ GeV}, \\ G_{\text{F}} &= 1.166379 \times 10^{-5} \text{ GeV}^{-2}, & \Gamma_Z &= 2.4952 \text{ GeV}. \end{aligned} \tag{3.1}$$

Unless otherwise stated, we use MSTW2008 parton distribution functions [65] with $\alpha_s(M_Z) = 0.13939$ and $\alpha_s(M_Z) = 0.12018$ at LO and NLO, which we evolve to the renormalization scale μ_{ren} using 1-loop and 2-loop running, respectively. The LO and NLO scale dependence has already been studied in previous works, we therefore do not repeat these studies here and adopt the central scale [21] $\mu_0 = m_t + M_Z/2$ for $\mu = \mu_{\text{ren}} = \mu_{\text{fact}}$. Since we include

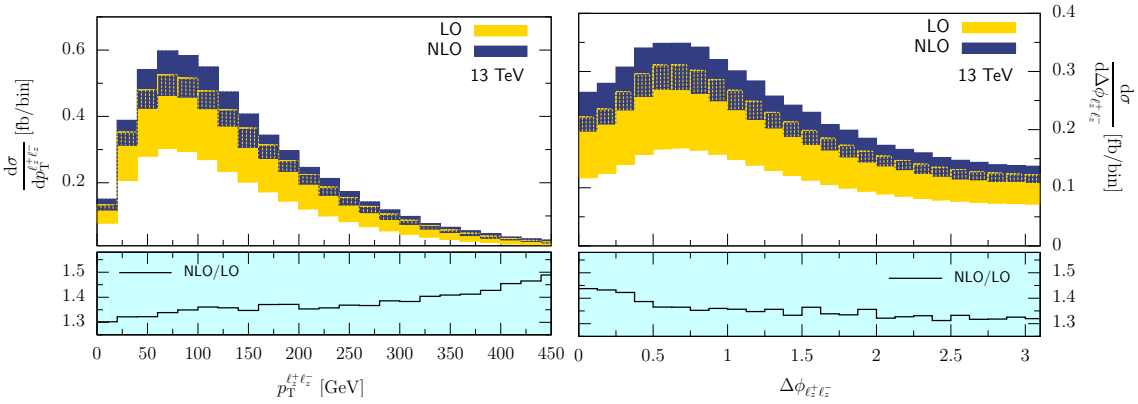

Figure 2: Transverse momentum spectrum (left) and azimuth opening angle (right) of the two leptons from the Z boson in the process $pp \to t\bar{t} + Z \to t(\to \ell\nu b)\,\bar{t}(\to jj\bar{b})\,Z(\to \ell\ell)$ at the 13 TeV LHC. The bands represent the LO (light) and NLO (dark) results for scale variation by a factor of two around the central scale μ_0. The lower panes show the differential K-factors.

NLO QCD corrections to the top quark decay and the hadronically decaying W boson, we need to include their total widths up to next-to-leading order,

$$\begin{aligned} \Gamma_t^{\rm LO} &= 1.4957 \text{ GeV}, \quad \Gamma_t^{\rm NLO} = 1.3693 \text{ GeV}, \\ \Gamma_W^{\rm LO} &= 2.0455 \text{ GeV}, \quad \Gamma_W^{\rm NLO} = 2.1145 \text{ GeV}. \end{aligned} \tag{3.2}$$

We consider proton-proton collisions at the LHC with a center-of-mass energy of $\sqrt{s} = 13$ TeV. To account for detector acceptances and trigger we require

$$\begin{aligned} p_{\rm T}^{\ell} &\geq 15 \text{ GeV}, \quad |y^{\ell}| \leq 2.5, \\ p_{\rm T}^{j} &\geq 20 \text{ GeV}, \quad |y^{j}| \leq 2.5, \\ p_{\rm T}^{\rm miss} &\geq 20 \text{ GeV}, \quad R_{\ell j} \geq 0.4. \end{aligned} \tag{3.3}$$

Jet are defined by the anti-$k_{\rm T}$ algorithm [66] with $R = 0.4$. With these input parameter and cuts we find the LO and NLO QCD cross sections,

$$\sigma_{t\bar{t}Z}^{\rm LO} = 3.79(0)^{+34\%}_{-25\%} \text{ fb}, \qquad \sigma_{t\bar{t}Z}^{\rm NLO} = 5.16(1)^{+13\%}_{-12\%} \text{ fb} \tag{3.4}$$

for the central scale μ_0 which is varied by factors of 2 and 1/2, the value in bracket is the integration error on the last digit. The dependence on the unphysical scale is reduced from approximately $\pm 30\%$ at LO to $\pm 13\%$ at NLO QCD. Higher order corrections increase the cross section by 36%, $K = \sigma_{t\bar{t}Z}^{\rm NLO}/\sigma_{t\bar{t}Z}^{\rm LO} = 1.36$. We also calculate the cross sections without any acceptance cuts and find a significantly lower $K = 1.23$. This emphasizes the importance of modeling a realistic final state with all unstable particles decayed. The ratio of the cross sections with and without cuts defines the acceptance function A, we find

$$A^{\rm LO} = \frac{\sigma_{\rm cuts}^{\rm LO}}{\sigma_{\rm total}^{\rm LO}} = 27.1\%, \qquad A^{\rm NLO} = \frac{\sigma_{\rm cuts}^{\rm NLO}}{\sigma_{\rm total}^{\rm NLO}} = 30.0\%. \tag{3.5}$$

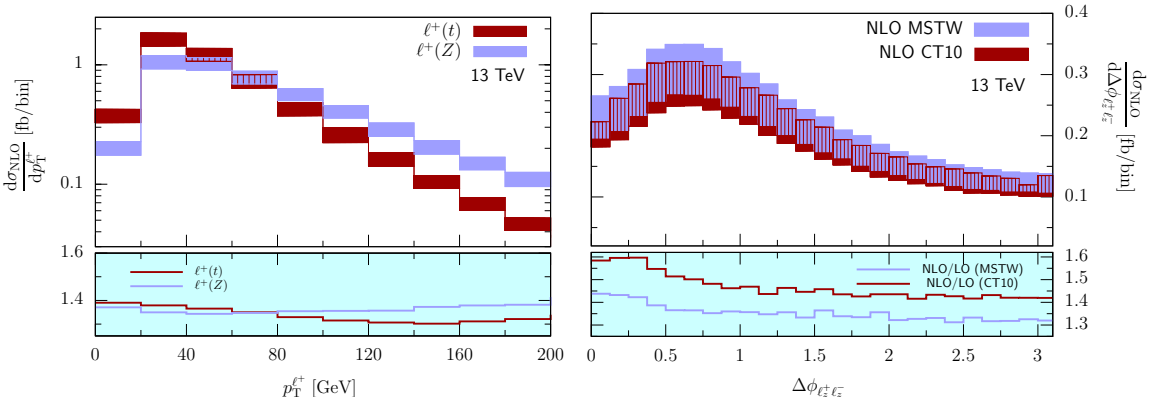

Figure 3: Left: Comparison of transverse momenta of leptons arising from the top quark decay (dark) and the Z boson (light) in the process $pp \to t\bar{t} + Z \to t(\to \ell\nu b)\,\bar{t}(\to jj\bar{b})\,Z(\to \ell\ell)$ at NLO QCD. Right: Comparison of NLO predictions using two different pdf sets (MSTW light, CTEQ dark) for the azimuth opening angle of the two leptons from the Z boson. The lower panes show the differential K-factors.

The increase of approximately +3% when going from leading to next-to-leading order seems minor. However, the common practice of modeling acceptance effects at LO and multiplying with a K-factor obtained from a NLO calculation with stable particles, underestimates the correct NLO cross section by $\sim 1 - A^{\rm LO}/A^{\rm NLO} = 10\%$. To estimate uncertainties from parton distribution functions we contrast the results in Eq. (3.4) (MSTW pdfs [65]) with a calculation that uses the pdf sets from CTEQ6L1 [52] and CT10 [67] at LO and NLO QCD, respectively. We find

$$\sigma^{\rm LO}_{t\bar{t}Z} = 3.25(0)^{+34\%}_{-23\%}\ \text{fb}, \qquad \sigma^{\rm NLO}_{t\bar{t}Z} = 4.80(1)^{+13\%}_{-13\%}\ \text{fb}. \tag{3.6}$$

These cross sections are about 14% smaller at LO and 7% smaller at NLO QCD compared to the results obtained with MSTW parton distribution functions. At NLO, we find that 4% out of the total difference of 7% is due to the different values of $\alpha_s(M_Z)$. The resulting scale uncertainty bands are approximately the same for CTEQ and MSTW pdfs. Hence, the difference due to two different parton distribution sets is well within the uncertainty estimate from factorization and renormalization scales.

Before turning to the $t\bar{t}Z$ coupling analysis, let us discuss some generic kinematic distributions. Fig. 2(left) shows the transverse momentum of the two lepton system reconstructing the Z boson. Similar to the total cross sections we observe a strong reduction in unphysical scale dependence over the entire $p_{\rm T}$ spectrum. Scale bands for LO and NLO predictions are comfortably overlapping. From this plot we read off an average transverse momentum of the Z boson of almost 100 GeV with a far extending kinematic tail, promising approximately 30 events with $p_{\rm T}^Z \approx 300$ GeV from 300 fb^{-1} at the 13 TeV LHC. Fig. 2(right) shows the azimuth opening angle between the two leptons from the Z boson decay. This observable has been proven to be a good analyzer of the $t\bar{t}Z$ couplings [18] and we will consider it in the following analysis. Also here, we observe a strong reduction in scale dependence when going from LO to NLO. The differential K-factor in the lower pane of this plot shows shape changes in the range of 10 % due to higher order corrections.

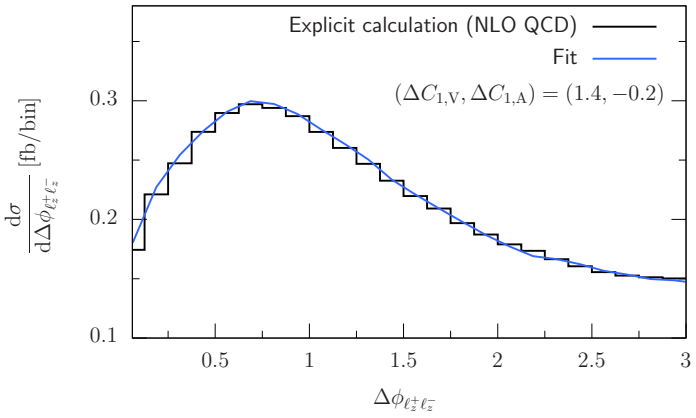

Figure 4: Validation of our fitting procedure. Shown is the $\Delta\phi_{\ell_z^+\ell_z^-}$ distribution from an explicit NLO QCD calculation for the non-SM coupling choice $(\Delta C_{1,\mathrm{V}}, \Delta C_{1,\mathrm{A}}) = (1.4, -0.2)$, and from the fit described in Eq. (3.8).

On the left hand side of Fig. 3 we compare the transverse momentum spectra (at NLO QCD) of the leptons arising from either the top quark decay or the Z boson. It turns out that below transverse momenta of about 50 GeV the leptons from W boson in the top quark decay are harder than the ones from the Z boson. At higher energies a turnover happens and the leptons from the Z boson decay become significantly harder. In Fig. 3(right) we study the dependence of our predictions on different parton distribution sets. The results for the $\Delta\phi_{\ell_z^+\ell_z^-}$ distribution show that the two NLO predictions obtained with MSTW [65] and CTEQ [52, 67] pdfs yield consistent results over the entire spectrum. However, as can be seen in the lower pane, the K-factors differ significantly (10% or more) due to very different prediction with LO pdfs (cf. also Eqs. (3.4) and (3.6)).

3.2 Coupling extrapolation and statistical analysis

We will now use our calculation to investigate the constraints that can be placed on $t\bar{t}Z$ couplings, using both existing and anticipated LHC data. To do so, we need to determine how normalization and shapes of differential distributions depend on variations of the couplings. Hence total cross sections and differential distributions need to be calculated for a large grid of $C_{1,V}$ and $C_{1,A}$ values. This is simple enough at LO, and while it is still feasible at NLO, it does place a strain on computing resources. As a convenient alternative, we note that $t\bar{t}Z$ production and decay amplitude at LO or NLO QCD can be written as

$$\mathcal{M} = \mathcal{M}_0 + C_{1,\mathrm{V}}\mathcal{M}_\mathrm{V} + C_{1,\mathrm{A}}\mathcal{M}_\mathrm{A}, \tag{3.7}$$

with the coefficients $\mathcal{M}_i$ encoding both the kinematics and all couplings other than the $t\bar{t}Z$ couplings. The differential cross section is then dependent on six coupling structures, and can be written as

$$d\sigma = s_0 + s_1 C_{1,V} + s_2 C_{1,V}^2 + s_3 C_{1,A} + s_4 C_{1,A}^2 + s_5 C_{1,V} C_{1,A}. \tag{3.8}$$

Evaluating the cross section for six values of $(C_{1,V}, C_{1,A})$ allows us to solve for the coefficients s_i. These can then be used to extrapolate results for any values of $C_{1,V}$ and $C_{1,A}$.

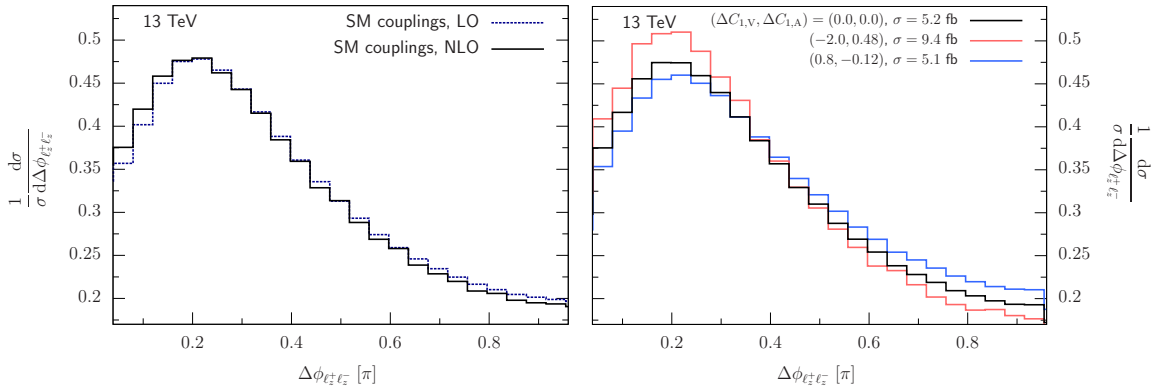

Figure 5: Normalized distributions of the azimuth opening angle of the opposite sign leptons from the Z boson decay at the 13 TeV LHC. In the left figure, shapes of LO and NLO QCD predictions are compared for SM $t\bar{t}Z$-couplings. Shape changes due to deviations from the SM values are shown in the right figure.

Furthermore, this fitting procedure can not only be done for the total cross section but also bin-by-bin for a given distribution, retaining the effects of spin correlations and selection cuts. As a check of this approach, we have evaluated the cross sections and distributions for a few points in the $(C_{1,V}, C_{1,A})$ parameter space, both by an explicit calculation and by using the fit for the s_i coefficients. Excellent agreement is found in all cases. As an example, we show one comparison in Fig. 4 for the $\Delta\phi_{\ell_z^+\ell_z^-}$ distribution, which we will later use in the coupling analysis. As can be seen in Fig. 4, the overall normalization and the shape are correctly reproduced by the fitting procedure. The relative shifts in the couplings are given by

$$\Delta C_{1,\mathrm{V}} = \frac{C_{1,\mathrm{V}}}{C_{\mathrm{V}}^{\mathrm{SM}}} - 1, \qquad \Delta C_{1,\mathrm{A}} = \frac{C_{1,\mathrm{A}}}{C_{\mathrm{A}}^{\mathrm{SM}}} - 1. \tag{3.9}$$

In our analysis we focus on the tri-leptonic final state and employ the azimuth angle between the leptons originating from the Z decay to perform our analysis. This angle has been identified as being particularly sensitive to the $t\bar{t}Z$ couplings in Ref. [18]. We already discussed the strong reduction in scale uncertainty when going from LO to NLO QCD for this observable. Here, in Fig. 5(left), we show the effect of NLO QCD corrections on the shape of the normalized $\Delta\phi_{\ell\ell}$ distribution. Higher order effects tend to shift events from larger to smaller opening angles. In Fig. 5(right) we show that similar shape changes can arise due to variations of the vector and axial $t\bar{t}Z$-couplings. This emphasizes the importance of precise predictions since missing higher order effects might be misinterpreted as deviations from the SM. To illustrate that the $\Delta\phi_{\ell\ell}$ shape is a useful discriminator for our coupling analysis, we have chosen a value $(\Delta C_{1,\mathrm{V}}, \Delta C_{1,\mathrm{A}})$ in Fig. 5(right) such that the total cross sections approximately coincide with the SM $t\bar{t}Z$ cross section. Hence, a measurement of the rate alone would not reveal the deviations from its Standard Model value.

Let us now outline the basic features of our statistical analysis. We are interested in answering the question: What are the bounds that can be placed on deviations of the $t\bar{t}Z$ couplings, assuming that the SM is true. Obviously, the answer will depend on the assumed integrated luminosity of the data sample as well as on theoretical and experimental uncertainties. We assume the SM prediction as our null hypothesis $\mathcal{H}_{\rm SM}$ $(\Delta C_{1,\rm V}, \Delta C_{1,\rm A}) = (0,0)$, against which we test alternative hypotheses $\mathcal{H}_{\rm alt}$ with $(\Delta C_{1,\rm V}, \Delta C_{1,\rm A}) \neq (0,0)$. Alternatively, the null hypothesis can be replaced by observed data from LHC experiments to determine the best fit in $(\Delta C_{1,\rm V}, \Delta C_{1,\rm A})$ parameter space. This also enables the exclusion of parts of the parameter space at a given confidence level. Assuming that the data agree with the SM, the bounds on the $t\bar{t}Z$ couplings obtained in this section should approximate those obtained from real data. We construct two likelihood functions $\mathcal{L}_{\rm SM}$ and $\mathcal{L}_{\rm alt}$ which allow us to define a test statistic $\Lambda = \log\left(\mathcal{L}_{\rm SM}/\mathcal{L}_{\rm alt}\right)$. We then generate two event samples for a fixed integrated luminosity assuming that either $\mathcal{H}_{\rm SM}$ or $\mathcal{H}_{\rm alt}$ is true. The test statistic Λ can be evaluated for these two event samples, and repeating this evaluation in a large number of pseudo experiments provides the probability distributions $P(\Lambda|\mathcal{H}_{\rm SM})$ or $P(\Lambda|\mathcal{H}_{\rm alt})$. The overlap of these two probability distributions can be used to define the type-I error for rejecting $\mathcal{H}_{\rm SM}$ in favor of $\mathcal{H}_{\rm alt}$, even though $\mathcal{H}_{\rm SM}$ is true. This error can finally be translated into the more familiar confidence level in terms of standard deviations.

Let us now describe the procedure outlined above more precisely and illustrate how differential distributions at NLO QCD can be used. We closely follow typical likelihood-based analysis as described for example in Ref. [68], based on the original procedure by Feldman and Cousins [69]. The starting point is the binned likelihood function

$$\mathcal{L}(\mathcal{H}|\vec{n}) = \prod_{i=1}^{N_{\rm bins}} P_i(n_i|\nu_i^{\mathcal{H}}) \tag{3.10}$$

with the Poisson distribution P_i for n_i events in the i-th bin, given the expected value $\nu_i^{\mathcal{H}}$ for hypothesis $\mathcal{H}$. Consequently the two log-likelihood functions for the SM and the alternative hypothesis read

$$\begin{aligned}
\log\mathcal{L}(\mathcal{H}_{\rm SM}|\vec{n}_{\rm obs}) &= \sum_{i=1}^{N_{\rm bins}} \left[n_{i,\rm obs}\log(\nu_i^{\rm SM}) - \log(n_{i,\rm obs}!) - \nu_i^{\rm SM}\right], \\
\log\mathcal{L}(\mathcal{H}_{\rm alt}|\vec{n}_{\rm obs}) &= \sum_{i=1}^{N_{\rm bins}} \left[n_{i,\rm obs}\log(\nu_i^{\rm alt}) - \log(n_{i,\rm obs}!) - \nu_i^{\rm alt}\right],
\end{aligned} \tag{3.11}$$

where the sums over i runs over all bins in a given histogram. Eqs. (3.11) allow us to construct a log-likelihood ratio which serves as the test statistic

$$\begin{aligned}
\Lambda(\vec{n}_{\rm obs}) &= \log\left(\mathcal{L}(\mathcal{H}_{\rm SM}|\vec{n}_{\rm obs})/\mathcal{L}(\mathcal{H}_{\rm alt}|\vec{n}_{\rm obs})\right) \\
&= \sum_{i=1}^{N_{\rm bins}} \left[n_{i,\rm obs}\log\left(\frac{\nu_i^{\rm SM}}{\nu_i^{\rm alt}}\right) - \nu_i^{\rm SM} + \nu_i^{\rm alt}\right].
\end{aligned} \tag{3.12}$$

This test statistic can now be evaluated with $\vec{n}_{\rm obs}$ which are the Poisson distributed events from the $\Delta\phi_{\ell\ell}$ histogram, for either the SM or the alternative hypothesis. Repeating this

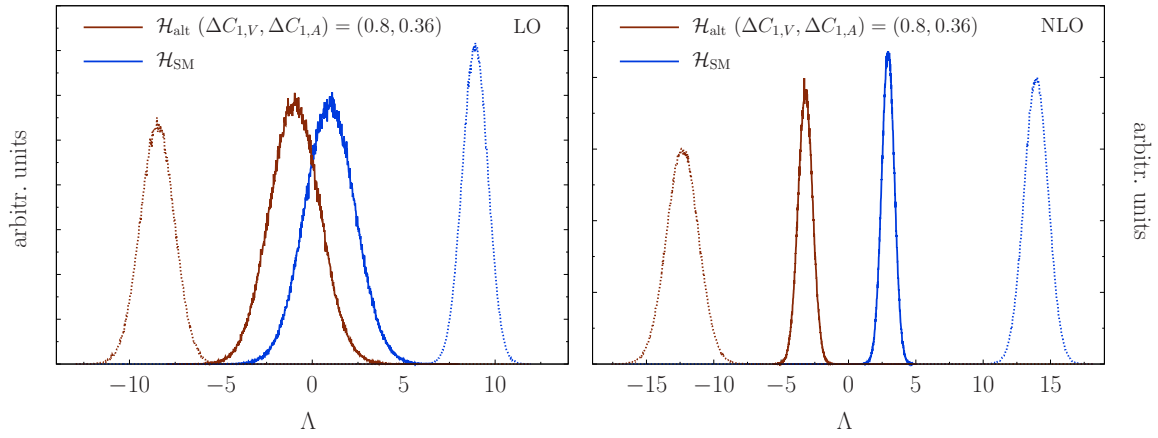

Figure 6: Probability distributions of the log-likelihood ratio Λ assuming that the observed events follow the SM hypothesis (red) or an alternative hypothesis (blue) with $(\Delta C_{1,\rm V}, \Delta C_{1,\rm A}) = (0.8, 0.36)$. The solid lines include statistic and systematic uncertainties as described in the text, whereas the dashed lines only include statistic uncertainties. The left plot shows the separating power using LO input with $\Delta_{\rm syst.} = 30\%$, the right plot is obtained at NLO QCD with $\Delta_{\rm syst.} = 15\%$, assuming $\sqrt{s} = 13\,\text{TeV}$ and $\mathcal{L} = 300\,\text{fb}^{-1}$.

procedure for a large number of pseudo-experiments yields the two probability distributions of $\Lambda(\vec{n}_{\rm SM})$ and $\Lambda(\vec{n}_{\rm alt})$. An example of two such probability distributions, $P(\Lambda|\mathcal{H}_{\rm SM/alt})$, is shown in Fig. 6 for LO (left) and NLO QCD (right). These two distributions can be used to define a confidence level for excluding the alternative hypothesis. For a given value $\hat{\Lambda}$, the probability of accepting $\mathcal{H}_{\rm alt}$ even though $\mathcal{H}_{\rm SM}$ is correct (type-I error) is

$$\alpha = \int_{-\infty}^{\hat{\Lambda}} \mathrm{d}\Lambda\; P(\Lambda|\mathcal{H}_{\rm SM}). \tag{3.13}$$

Similarly, the probability of accepting $\mathcal{H}_{\rm SM}$ even though $\mathcal{H}_{\rm alt}$ is correct (type-II error) is given as

$$\beta = \int_{\hat{\Lambda}}^{\infty} \mathrm{d}\Lambda\; P(\Lambda|\mathcal{H}_{\rm alt}). \tag{3.14}$$

We define $\hat{\Lambda}$ such that $\alpha = \beta$, i.e. there is equal chance of *incorrectly* rejecting one hypothesis in favor of the other. The value $\alpha(\hat{\Lambda})$ is then a measure of statistical discrimination between the two hypotheses. It can be translated into the more familiar number of standard deviations by

$$\sigma = \sqrt{2}\,\mathrm{erf}^{-1}(1-\alpha), \tag{3.15}$$

where erf^{-1} is the inverse error function.

The above discussion made so far no mention of systematic uncertainties. In this work we would like to include the leading theoretical uncertainties from unphysical scale dependence and errors associated with parton distribution functions. For simplicity we neglect experimental systematics such as efficiencies or momentum smearing effects. Note however that we include realistic detector acceptances through the cuts in Eq. (3.3). Statistical fluctuations are obviously included in our analysis through the Poisson distribution

in Eq. (3.10). Following Ref. [70], we include the theoretical uncertainties through nuisance parameters by multiplicative factors. At this point we should mention that the use of a log-likelihood ratio as test statistic is guaranteed to be optimal thanks to the Neyman-Pearson lemma [71]. This is however no longer true when nuisance parameters are introduced in the analysis. Nevertheless, one still expects the test to be approximately optimal as long as the nuisance parameters are reasonably constrained. We include the theoretical uncertainties by modifying the likelihood function in Eq. (3.10) according to

$$\mathcal{L}(\mathcal{H}|\vec{n}) \to \mathcal{L}(\mathcal{H}|\vec{n}) \times \mathcal{G}\left(\nu_i^{\mathcal{H}}|\tilde{\nu}_i^{\mathcal{H}}(\Delta_{\text{theor. unc.}})\right), \tag{3.16}$$

where we choose $\mathcal{G}$ to be a normalized function with uniform spread $\tilde{\nu}^{\mathcal{H}}_{\text{min/max},i} = \tilde{\nu}_i^{\mathcal{H}} \pm \Delta_{\text{theor. unc.}}$,

$$\mathcal{G}\left(\nu_i^{\mathcal{H}}|\tilde{\nu}_i^{\mathcal{H}}(\Delta_{\text{theor. unc.}})\right) = \left(\theta\left(\nu_i^{\mathcal{H}} - \nu^{\mathcal{H}}_{\text{min},i}\right) \times \theta\left(\nu^{\mathcal{H}}_{\text{max},i} - \nu_i^{\mathcal{H}}\right)\right) / \left(\nu^{\mathcal{H}}_{\text{max},i} - \nu^{\mathcal{H}}_{\text{min},i}\right). \tag{3.17}$$

The value of $\tilde{\nu}_i^{\mathcal{H}}$ is determined by the assumed luminosity times the cross section in the ith bin for the central scale choice μ_0. We will choose the constant values $\Delta_{\text{theor. unc.}} = 30\%$ at LO and $\Delta_{\text{theor. unc.}} = 15\%$ at NLO QCD for our $\sqrt{s} = 13$ TeV analysis below. To be most conservative, we then fix $\nu_i^{\mathcal{H}}$ to either $\tilde{\nu}^{\mathcal{H}}_{\text{min},i}$ or $\tilde{\nu}^{\mathcal{H}}_{\text{max},i}$ for the respective hypothesis such that their total cross sections are closest. This treatment results in a larger overlap between the two likelihood distributions, and consequently a larger α value and less discriminatory power between the two hypotheses. This feature is clearly visible in Fig. 6, when comparing the solid with the doted curves. Contrasting the LO results in Fig. 6(left) with the NLO result (right) shows that the lower uncertainty associated with the NLO prediction allows for significantly better statistical discrimination between the hypotheses. Also the increase of the NLO cross section due to the K-factor of ≈ 1.4 leads to a larger number of expected events and therefore to smaller statistical uncertainties.

3.3 $t\bar{t}Z$ coupling constraints from current and future LHC data

We now apply the analysis outlined in the previous section to study coupling constraints from current and future LHC data. Figure 7 shows the relative shift of the $t\bar{t}Z$ cross section for non-SM couplings wrt. the SM cross section for a wide range of vector and axial couplings. The grid of 3200 NLO QCD cross sections is generated with the fit described in Eq. (3.8), at low computational cost, and accounts for selection cuts of Eq. (3.3). We find that within the given range the cross sections vary by about $\pm 50\%$ away from the SM value due to shifts of vector and axial couplings. The remaining scale uncertainty at NLO QCD was found to be $\pm 13\%$ which roughly corresponds to the area enclosed by the dotted line in Fig. 7. Hence, for all coupling values within this band a rate measurement alone is not sensitive to any deviation. This is true for a large range of couplings far off the SM value, e.g. $(\Delta C_{1,\text{V}}, \Delta C_{1,\text{A}}) = (1.7, -0.3)$. We will later see that adding shape information from kinematic distributions will improve this situation and lead to a more powerful discrimination. It is clearly noticeable in Fig. 7 that cross sections are symmetric around the axis $\Delta C_{1,\text{V}} = -1$. This feature can be easily understood from the fact that the LO cross section is dominantly proportional to $C_{1,\text{V}}^2 + C_{1,\text{A}}^2$ and $\Delta C_{1,\text{V}} = -1$ corresponds

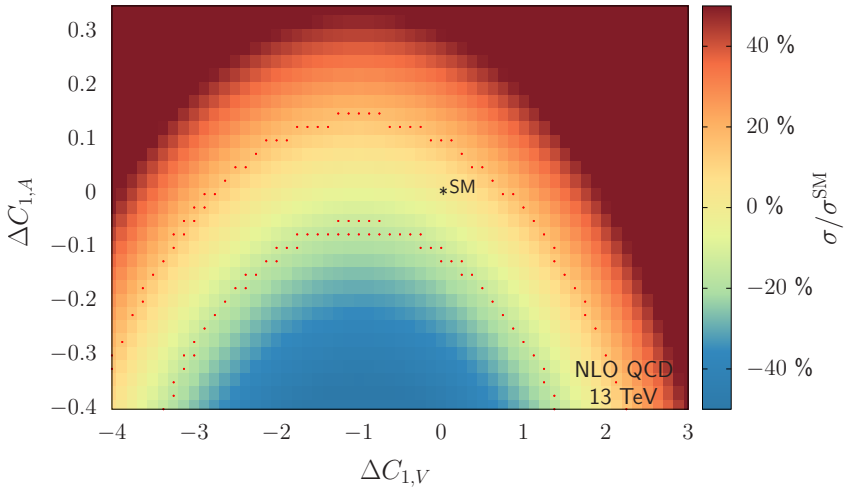

Figure 7: Relative deviations of the NLO QCD cross section as a function of relative shifts in vector and axial couplings wrt. the SM. The grid of 80×40 coupling choices is obtained from the fit described in Eq. (3.8).

to the point $C_{1,\mathrm{V}} = 0$. We expect to see a similar symmetry around $\Delta C_{1,\mathrm{A}} = -1$ but we do not consider it here since the sign of the axial coupling is already constrained from LEP measurements of the $Zb_{\mathrm{L}}\bar{b}_{\mathrm{L}}$ interaction when $\mathrm{SU}(2)_{\mathrm{L}}$ symmetry is invoked.

As a side remark we would like to briefly note that we also studied the effects of $t\bar{t}Z$ coupling shifts on the top quark forward-backward asymmetry ($A_{\mathrm{FB}}^{t\bar{t}}$) at the Tevatron. At leading order, we considered the parity-violating process $q\bar{q} \to Z/\gamma^* \to t\bar{t}$ with coupling variations as shown in Fig. 7. We find that within this range the forward-backward asymmetry is not significantly enhanced. Hence, current discrepancies between theory and experiment for $A_{\mathrm{FB}}^{t\bar{t}}$ cannot be explained by deviations of the $t\bar{t}Z$ couplings as assumed in this paper.

Let us now use current LHC data to obtain first direct constraints on vector and axial couplings. The production of $t\bar{t}Z$ has been observed at the $\sqrt{s} = 7$ TeV run at the LHC, with CMS observing nine events [6], and ATLAS observing one event with more stringent selection criteria [5]. This enables ATLAS to place an upper bound on the $t\bar{t}Z$ cross section, while CMS is able to determine $\sigma_{t\bar{t}Z}^{\mathrm{CMS}} = 0.28^{+0.14}_{-0.11}\ (\mathrm{stat.})^{+0.06}_{-0.03}\ (\mathrm{sys.})$ pb. Clearly, error bars from this very first measurement are large, nevertheless it constitutes a 3.3 standard deviation from the background-only hypothesis. The measured total cross section is also consistent with the NLO QCD predictions of $0.137\,\mathrm{pb} \pm 11\%$ by Ref. [23] (CTEQ pdfs) or with $0.148\,\mathrm{pb} \pm 11\%$ from our calculation (MSTW pdfs). In spite of the low number of events and correspondingly high statistical error, it is instructive to use this measured cross section to place bounds on the $t\bar{t}Z$ couplings. This constitutes the first direct constraints on these couplings. We perform a log-likelihood analysis, as described in Section 3.2. Our null hypothesis is derived from the experimental cross section $\sigma_{t\bar{t}Z}^{\mathrm{CMS}} = 0.28$ pb, from which we predict 24 events in the trilepton channel from 5 fb^{-1} of data if no acceptance cuts are applied. We are adopting this number as our reference point against which we compare the alternative hypothesis. As described before, it is obtained from our theoretical

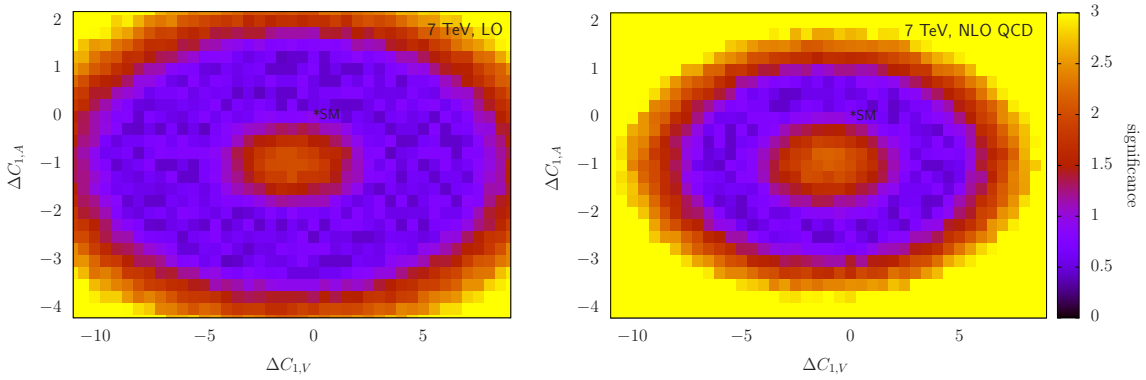

Figure 8: Significance as a function of relative deviations for vector and axial couplings wrt. the SM value. The limits are obtained from the first measurement of the $t\bar{t}Z$ cross section by CMS [6]. The left (right) plot shows the limits obtained from LO (NLO QCD) input.

prediction for various points in $(C_{1,\mathrm{V}}, C_{1,\mathrm{A}})$ parameter space. To account for uncertainties we include a uniform distribution spanned by the theoretical error band. Since we find slightly larger LO uncertainties for the pdfs at 8 TeV, we choose $\Delta_{\text{theor. unc.}} = 40\%$ at LO and keep $\Delta_{\text{theor. unc.}} = 15\%$ at NLO QCD. For experimental systematics we need to introduce a Gaussian distributed probability. Hence, the function $\mathcal{G}(..|..)$ in Eq. (3.16) has to be modified and becomes

$$\mathcal{G}\left(\nu|\tilde{\nu},\tilde{\sigma}\right) = \frac{1}{\sqrt{2\pi\tilde{\sigma}^2}}\, e^{-(\nu-\tilde{\nu})^2/(2\tilde{\sigma}^2)}, \tag{3.18}$$

where $\tilde{\nu}$ is the mean value of the experimental measurement and $\tilde{\sigma} = \sigma_{\text{exp. syst.}}$ is the systematic experimental uncertainty. In this way the mean value ν in the likelihood function is normal distributed during the generation of pseudo experiments with a standard deviation of $\sigma_{\text{exp. syst.}}$. We adopt the experimental systematic error of $\sigma_{\text{exp. syst.}} = \pm 20\%$ quoted in Ref. [6]. The results of the log-likelihood ratio test are shown in Figure 8, for our LO (left) and NLO (right) calculations. The color code shows the significance with which an alternative coupling hypothesis can be excluded wrt. to the experimental data. In the plane of relative deviations of vector and axial couplings, the point $(\Delta C_{1,\mathrm{V}}, \Delta C_{1,\mathrm{A}}) = (0.0, 0.0)$ corresponds to the SM value. Clearly, this point is fully consistent with the experimental measurement. By comparing left and right plots we notice the stronger constraints when NLO input is used. The constraints from the data using a LO calculation are $-11 \lesssim \Delta C_{1,\mathrm{V}} \lesssim 10$ and $-4 \lesssim \Delta C_{1,\mathrm{A}} \lesssim 2$ at the 95% C.L., while they improve at NLO to $-8 \lesssim \Delta C_{1,\mathrm{V}} \lesssim 7$ and $-3 \lesssim \Delta C_{1,\mathrm{A}} \lesssim 1$. Of course, these limits are extremely loose, and furthermore should be interpreted with care since very few events have been observed by the experiments so far. Only a larger data set and detailed analysis of backgrounds and detector effects will provide more reliable constraints on the $t\bar{t}Z$-couplings. We still believe that these results are interesting to consider, especially when being put in context with limits obtained from the future high-energy LHC which we study in the next section.

We now present the main results of our analysis in Figs. 9 and 10 for the future run of the LHC at $\sqrt{s} = 13$ TeV. Using the interpolation of Eq. (3.8) we generate 441

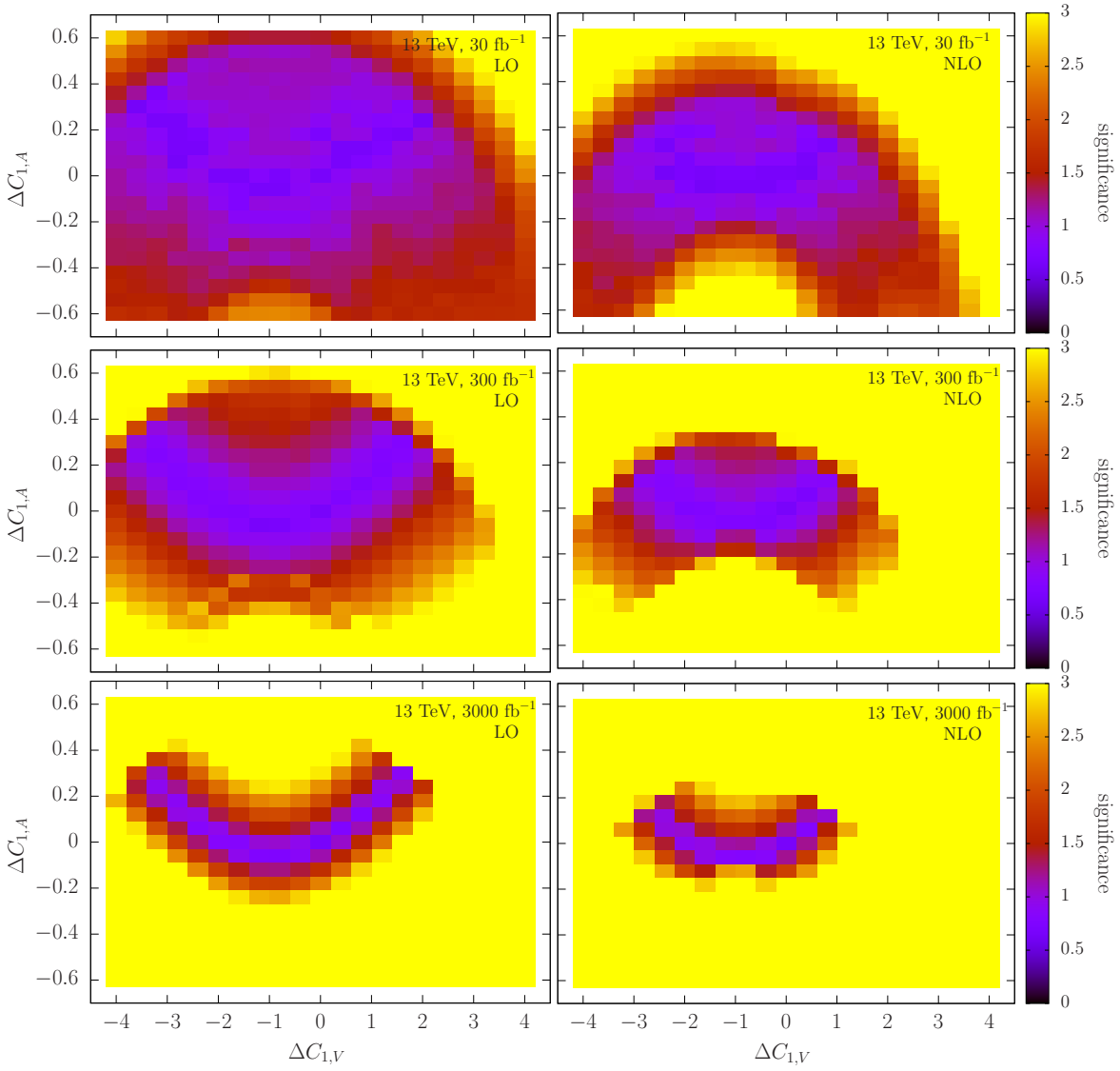

Figure 9: Significance of deviations from the SM vector and axial couplings $\Delta C_{1,\mathrm{V}}$ and $\Delta C_{1,\mathrm{A}}$, using 30, 300 and 3000 fb^{-1} of data at the $\sqrt{s} = 13$ TeV LHC. Results using the LO prediction and uncertainty are shown on the left, the corresponding NLO QCD results are shown on the right hand side.

distributions in $\Delta\phi_{\ell\ell}$ for a grid of 21×21 $\Delta C_{1,\mathrm{V}}, \Delta C_{1,\mathrm{A}}$ couplings choices in the range ± 4 and ± 0.6, respectively. In terms of absolute numbers, this corresponds to a variation between $[-0.732 \ldots 1.22]$ around $C_{\mathrm{V}}^{\mathrm{SM}} = 0.244$ and $[-0.962 \ldots -0.240]$ around $C_{\mathrm{A}}^{\mathrm{SM}} = -0.601$. The plots in Fig. 9 show the significance with which non-SM $t\bar{t}Z$ couplings can be separated from the SM hypothesis, assuming that the SM hypothesis is true. Clearly, this significance is a function of the accumulated luminosity and the associated uncertainties at the given order in perturbation theory. We therefore present six scenarios for luminosities of 30 fb^{-1}, 300 fb^{-1}, and 3000 fb^{-1} at the 13 TeV LHC with theory input at leading and next-to-leading order in QCD. As mentioned before, we assume total uncertainties of 30% at LO and 15%

at NLO. The couplings enclosed by the light-blue area in Fig. 9 roughly correspond to the ones that can be excluded at 68% confidence level (C.L.), whereas couplings inside the orange colored boundary can be excluded at 95% C.L. From comparing the first, second and third row of plots in Fig. 9 it is immediately apparent that increasing the luminosity drastically improves the limits. By comparing plots in the left versus the right column we also see that the bounds at NLO QCD are far stronger. This is a result of the reduced scale uncertainty and the larger cross section due to a positive perturbative correction at NLO. Numerically, one finds that with $300\,\text{fb}^{-1}$ and LO input $\Delta C_{1,\text{V}}$ is constrained between $[-4.0\,...\,2.8]$ and $\Delta C_{1,\text{A}}$ between $[-0.36\,...\,0.54]$, at the 95% C.L.[2] The limits improve with NLO QCD predictions to $[-3.6\,...\,1.6]$ for $\Delta C_{1,\text{V}}$ and $[-0.24\,...\,0.30]$ for $\Delta C_{1,\text{A}}$. In terms of absolute values, these intervals correspond to $C_\text{V} = 0.24^{+0.39}_{-0.39}$ and $C_\text{A} = -0.60^{+0.14}_{-0.18}$ at NLO QCD. This is a reduction by 25% and 42%, respectively, compared to results obtained at leading order. A noticeable feature in the exclusion limits at NLO, Fig. 9(right), is the turnover from a downwards bend shape to an upwards bend shape when going from $30\,\text{fb}^{-1}$ to $3000\,\text{fb}^{-1}$. This feature is a convoluted effect of our uncertainty treatment and a transition from normalization to shape sensitivity in the exclusion. In the upper right plot the exclusion region roughly follows the shape already observed in Fig. 7. This can be understood from the fact that with a small event sample the exclusion limit is dominated by normalization differences, whereas different shapes have vanishing exclusion power. Using a larger event sample, shape sensitivity increases and also allows to exclude regions where normalization differences are small but shapes differ significantly. This is the case in the lower right plot of Fig. 9, where the previously downwards bend are is safely excluded.

3.4 Limits on dimension-six operators

Having presented our main results in Fig. 9, we can use the obtained limits to put constraints on possible effects of physics beyond the SM. The relevant dimension-six operators have been presented in Sect. 2.2. This is also where we pointed out that the excellent agreement between experiment and prediction for the $Zb_\text{L}\bar{b}_\text{L}$ couplings can be used (together with $\text{SU}(2)_\text{L}$ symmetry of the SM) to relate $C_{\phi q}^{(3,33)} \approx -C_{\phi q}^{(1,33)}$. In the following we will make use of this fact and eliminate $C_{\phi q}^{(1,33)}$ from our analysis [3]. Hence we are left with only two dimension-six operators, $C_{\phi q}^{(3,33)}$ and $C_{\phi u}^{33}$. We begin by using the total cross section measurement of CMS at 7 TeV (see Sect. 3.3). The limits on the total $t\bar{t}Z$ cross section as a function of $\Delta C_{1,\text{V}}$ and $\Delta C_{1,\text{A}}$ directly translate into limits on the two operators. Diagonalizing the dependence in Eq. (2.6), we find at next-to-leading order

$$\begin{aligned} -2.6 \leq \quad & \tfrac{v^2}{\Lambda^2}\,\text{Re}\left[C_{\phi q}^{(3,33)}\right] \quad \leq 1.6, \\ -4.1 \leq \quad & \tfrac{v^2}{\Lambda^2}\,\text{Re}\left[C_{\phi u}^{33}\right] \quad \leq 4.1. \end{aligned} \tag{3.19}$$

[2] We checked that these LO limits roughly agree with the ones quoted in Ref. [18] for the 14 TeV LHC.

[3] It should be noted however that models exist which give vanishing corrections to $Zb\bar{b}$ for finite $C_{\phi q}^{(3,33)} + C_{\phi q}^{(1,33)}$. One example is given in Ref. [72] with vector-like quarks. In such case, our limits remain valid upon the replacement $C_{\phi q}^{(3,33)} \to C_{\phi q}^{(3,33)} - C_{\phi q}^{(1,33)}$.

This result should be considered with care given the low number of events observed in experiments. More reliable and stringent limits are only obtained once more data is accumulated. To estimate how limits will improve in such a case, we use the results presented in Fig. 9 for the luminosities 30, 300, and 3000 fb^{-1}. Note that these results are not only based on the total cross section but also on the shapes of the $\Delta\phi_{\ell_z^+\ell_z^-}$ distribution. We find at leading order

$$\left.\begin{matrix}-1.2\\-1.0\\-0.9\end{matrix}\right\} \leq \frac{v^2}{\Lambda^2}\,\mathrm{Re}\left[C_{\phi q}^{(3,33)}\right] \leq \begin{cases}1.0 & \text{with } 30\,\text{fb}^{-1}\\ 0.7 & \text{with } 300\,\text{fb}^{-1}\\ 0.6 & \text{with } 3000\,\text{fb}^{-1}\end{cases},$$
$$\left.\begin{matrix}-2.3\\-1.4\\-0.9\end{matrix}\right\} \leq \frac{v^2}{\Lambda^2}\,\mathrm{Re}\left[C_{\phi u}^{33}\right] \leq \begin{cases}2.2 & \text{with } 30\,\text{fb}^{-1}\\ 2.2 & \text{with } 300\,\text{fb}^{-1}\\ 2.0 & \text{with } 3000\,\text{fb}^{-1}\end{cases}. \tag{3.20}$$

At next-to-leading order QCD the limits improve to

$$\left.\begin{matrix}-1.2\\-0.9\\-0.7\end{matrix}\right\} \leq \frac{v^2}{\Lambda^2}\,\mathrm{Re}\left[C_{\phi q}^{(3,33)}\right] \leq \begin{cases}0.6 & \text{with } 30\,\text{fb}^{-1}\\ 0.4 & \text{with } 300\,\text{fb}^{-1}\\ 0.2 & \text{with } 3000\,\text{fb}^{-1}\end{cases},$$
$$\left.\begin{matrix}-1.7\\-0.8\\-0.4\end{matrix}\right\} \leq \frac{v^2}{\Lambda^2}\,\mathrm{Re}\left[C_{\phi u}^{33}\right] \leq \begin{cases}2.0 & \text{with } 30\,\text{fb}^{-1}\\ 1.8 & \text{with } 300\,\text{fb}^{-1}\\ 1.5 & \text{with } 3000\,\text{fb}^{-1}\end{cases}. \tag{3.21}$$

Due to the weak correlation between vector and axial coupling limits observed in Fig. 9 and because of Eq. (2.6), the limits on $C_{\phi q}^{(3,33)}$ and $C_{\phi u}^{33}$ are strongly correlated. Hence, the results in Eqs. (3.20)-(3.21) are very conservative. A more appropriate graphical representation of these limits is given in Fig. 10 for our NLO results. We also include the indirect constraints from electroweak precision observables ε_1 and ε_b [61–63], updated to account for $M_H = 125.6$ GeV in Ref. [60]. All effective operators outside the colored ellipse in Fig. 10 can be excluded at the 95% confidence level. We observe that the limits from $t\bar{t}Z$ production at the LHC are well-aligned with the precision limit from ε_1. This can be understood from the fact that ε_1 is directly proportional to the SM ρ-parameter which receives sensitivity from the Z boson self energy with a top quark loop insertion. The constraint from ε_b on the other hand arises from the measurement of $Z \to b\bar{b}$ and $\mathrm{SU(2)_L}$ symmetry of the SM. Hence it leaves $C_{\phi u}^{33}$ mostly unconstrained since this operator contributes to the right handed current only. Altogether, electroweak precision observables put very strong constraints on the $t\bar{t}Z$ coupling which, however, only arise through indirect sensitivity. Only the analysis of $pp \to t\bar{t}Z$ at the LHC will allow placing *direct* limits for the first time. It would be an interesting continuation of this work to superimpose Fig. 10 with constraints obtained from single $tZ + \bar{t}Z$ or single tW production at the LHC.

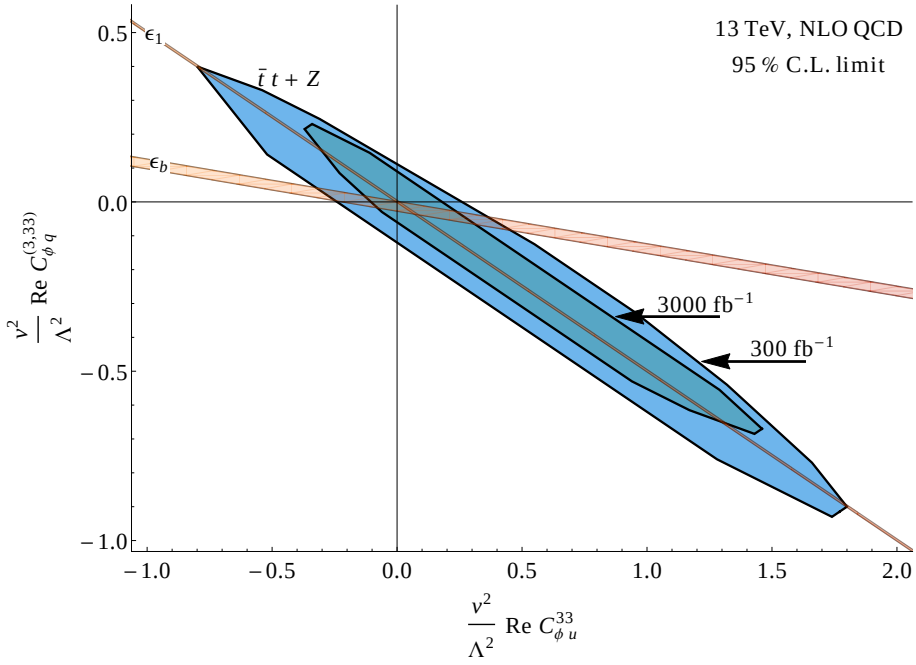

Figure 10: Projected constraints on the operators $C_{\phi q}^{(33,3)}$ and $C_{\phi u}^{33}$ obtained from the $\Delta\phi_{\ell_z^+\ell_z^-}$ distribution in $t\bar{t}Z$ production at the 13 TeV LHC. The parameter space outside the blue colored area can be excluded at the 95% C.L. The thin brown colored bands are indirect constraints from electroweak precision data.

4. Conclusion

In this article we studied top quark pair production in association with a Z boson. Due to its relatively high production threshold and penalties from small branching fractions this process was never observed at the Tevatron. Even at the 7 and 8 TeV run of the LHC only a few candidate events were collected. As a consequence there is no *direct* measurement of the top quark to Z boson couplings to this date. This situation will change once the high energy LHC delivers its first tens fb^{-1} of data. We therefore study the process $pp \to t\bar{t}Z$ at 13 TeV in the tri-lepton final state which provides the best compromise between clean signature and large enough cross section. The central question that we try to answer is by how much limits on $t\bar{t}Z$ couplings improve once NLO QCD predictions are used. A particularly sensitive observable for such a study is the opening angle between the two leptons from the Z boson decay. We perform the analysis with a binned log-likelihood ratio test which proves advantageous for several reasons. Firstly, the use of likelihood functions guarantees reliable results even for low number of events when, for example, a simple χ^2 analysis would fail. Secondly, non-Gaussian systematic errors such as theoretical scale uncertainties can be straightforwardly implemented in the likelihood ratio test. In addition it turns out relatively easy to implement this procedure at NLO QCD. To this end we generated a grid of 441 different couplings and their corresponding kinematic distributions at NLO QCD. Assuming a residual theoretical uncertainty of 15% at NLO we find that with 300 fb^{-1} of data the vector and axial couplings can be constrained to $C_{\mathrm{V}} = 0.24^{+0.39}_{-0.39}$

and $C_{\rm A} = -0.60^{+0.14}_{-0.18}$ at the 95% C.L. This is a significant improvement compared to an analysis at leading order. Even a first determination with only 30 fb^{-1} of data might be possible if NLO input is used, yielding limits which are about two times weaker. We also translate our constraints on vector and axial couplings into limits on dimension-six operators contributing to the $t\bar{t}Z$ couplings beyond the SM. The viable region for these operators can be significantly reduced with measurements of $pp \to t\bar{t}Z$ and $\mathcal{O}(100)$fb^{-1} of data. This allows to contrast high precision indirect limits from electroweak observables with a direct determination from the LHC.

Finally, we note that effects of New Physics can modify the $t\bar{t}Z$-coupling beyond vector and axial currents through q^2-dependent higher dimensional operators. Those couplings typically introduce non-renormalizable interactions and require an extension of our one-loop integrand reduction method. This is an interesting subject for a continuation of this work. Another interesting future topic is the study of sensitivity at an 100 TeV pp collider or at an e^+e^- machine. At any rate, we look forward to the first analysis of the $t\bar{t} + Z, W, \gamma, H$ processes and the consequential physics results in top quark phenomenology.

Acknowledgments

We acknowledge helpful conversations with P. Argrawal, Y. Gao and N. Tran. Some of the numeric calculations were done at NERSC.

References

[1] **CMS** Collaboration, S. Chatrchyan *et. al.*, *Observation of a new boson at a mass of 125 GeV with the CMS experiment at the LHC*, *Phys.Lett.* **B716** (2012) 30–61 [1207.7235].

[2] **ATLAS** Collaboration, G. Aad *et. al.*, *Observation of a new particle in the search for the Standard Model Higgs boson with the ATLAS detector at the LHC*, *Phys.Lett.* **B716** (2012) 1–29 [1207.7214].

[3] **ATLAS** Collaboration, *Measurement of the inclusive t tbar gamma cross section with the ATLAS detector*, .

[4] **CMS** Collaboration, *Measurement of the inclusive top-quark pair + photon production cross section in the muon + jets channel in pp collisions at 8 TeV*, .

[5] **ATLAS** Collaboration, *Search for $t\bar{t}Z$ production in the three lepton final state with* 4.7 fb^{-1} *of $\sqrt{s} = 7$ TeV pp collision data collected by the ATLAS detector*, Tech. Rep. ATLAS-CONF-2012-126, CERN, Geneva, Aug, 2012.

[6] **CMS** Collaboration, S. Chatrchyan *et. al.*, *Measurement of associated production of vector bosons and top quark-antiquark pairs at sqrt(s) = 7 TeV*, *Phys.Rev.Lett.* **110** (2013) 172002 [1303.3239].

[7] **ALEPH, DELPHI, L3 , OPAL, SLD, LEP Electroweak Working Group, SLD Electroweak Group, SLD Heavy Flavour Group** Collaboration, S. Schael *et. al.*, *Precision electroweak measurements on the Z resonance*, *Phys.Rept.* **427** (2006) 257–454 [hep-ex/0509008].

[8] **DELPHI** Collaboration, J. Abdallah *et. al.*, *A Study of b anti-b Production in e+e- Collisions at s**(1/2) = 130-GeV - 207-GeV*, *Eur.Phys.J.* **C60** (2009) 1–15 [0901.4461].

[9] W. Hollik, *Radiative Corrections in the Standard Model and their Role for Precision Tests of the Electroweak Theory*, *Fortsch.Phys.* **38** (1990) 165–260.

[10] T. Ibrahim and P. Nath, *Top quark electric dipole moment in a minimal supersymmetric standard model extension with vectorlike multiplets*, *Phys. Rev. D* **82** (Sep, 2010) 055001.

[11] T. Ibrahim and P. Nath, *Chromoelectric dipole moment of the top quark in models with vectorlike multiplets*, *Phys. Rev. D* **84** (Jul, 2011) 015003.

[12] M. Schmaltz, *Physics beyond the standard model (theory): Introducing the little Higgs*, *Nucl.Phys.Proc.Suppl.* **117** (2003) 40–49 [hep-ph/0210415].

[13] H.-C. Cheng and I. Low, *TeV symmetry and the little hierarchy problem*, *JHEP* **0309** (2003) 051 [hep-ph/0308199].

[14] P. H. Frampton, P. Hung and M. Sher, *Quarks and leptons beyond the third generation*, *Phys.Rept.* **330** (2000) 263 [hep-ph/9903387].

[15] B. A. Dobrescu, K. Kong and R. Mahbubani, *Prospects for top-prime quark discovery at the Tevatron*, *JHEP* **0906** (2009) 001 [0902.0792].

[16] R. S. Chivukula, P. Ittisamai, E. H. Simmons, B. Coleppa, H. E. Logan, A. Martin and J. Ren, *Discovering strong top dynamics at the lhc*, *Phys. Rev. D* **86** (Nov, 2012) 095017.

[17] L. Randall and R. Sundrum, *A Large mass hierarchy from a small extra dimension*, *Phys.Rev.Lett.* **83** (1999) 3370–3373 [hep-ph/9905221].

[18] U. Baur, A. Juste, L. Orr and D. Rainwater, *Probing electroweak top quark couplings at hadron colliders*, *Phys.Rev.* **D71** (2005) 054013 [hep-ph/0412021].

[19] U. Baur, A. Juste, D. Rainwater and L. Orr, *Improved measurement of ttZ couplings at the CERN LHC*, *Phys.Rev.* **D73** (2006) 034016 [hep-ph/0512262].

[20] E. L. Berger, Q.-H. Cao and I. Low, *Model Independent Constraints Among the Wtb, Zb anti-b, and Zt anti-t Couplings*, *Phys.Rev.* **D80** (2009) 074020 [0907.2191].

[21] A. Lazopoulos, T. McElmurry, K. Melnikov and F. Petriello, *Next-to-leading order QCD corrections to $t\bar{t}Z$ production at the LHC*, *Phys.Lett.* **B666** (2008) 62–65 [0804.2220].

[22] A. Kardos, Z. Trocsanyi and C. Papadopoulos, *Top quark pair production in association with a Z-boson at NLO accuracy*, *Phys.Rev.* **D85** (2012) 054015 [1111.0610].

[23] M. Garzelli, A. Kardos, C. Papadopoulos and Z. Trocsanyi, *Z0 - boson production in association with a top anti-top pair at NLO accuracy with parton shower effects*, *Phys.Rev.* **D85** (2012) 074022 [1111.1444].

[24] M. Garzelli, A. Kardos, C. Papadopoulos and Z. Trocsanyi, *$t\,\bar{t}\,W^{+-}$ and $t\,\bar{t}\,Z$ Hadroproduction at NLO accuracy in QCD with Parton Shower and Hadronization effects*, *JHEP* **1211** (2012) 056 [1208.2665].

[25] C. Buttar, J. D'Hondt, M. Kramer, G. Salam, M. Wobisch *et. al.*, *Standard Model Handles and Candles Working Group: Tools and Jets Summary Report*, 0803.0678.

[26] A. Denner, S. Dittmaier, S. Kallweit and S. Pozzorini, *NLO QCD corrections to off-shell top-antitop production with leptonic decays at hadron colliders*, *JHEP* **1210** (2012) 110 [1207.5018].

[27] G. Bevilacqua, M. Czakon, A. van Hameren, C. G. Papadopoulos and M. Worek, *Complete off-shell effects in top quark pair hadroproduction with leptonic decay at next-to-leading order*, *JHEP* **1102** (2011) 083 [1012.4230].

[28] G. Heinrich, A. Maier, R. Nisius, J. Schlenk and J. Winter, *NLO QCD corrections to WWbb production with leptonic decays in the light of top quark mass and asymmetry measurements*, 1312.6659.

[29] J. Campbell, R. K. Ellis and R. Rontsch, *Single top production in association with a Z boson at the LHC*, *Phys.Rev.* **D87** (2013) 114006 [1302.3856].

[30] G. Altarelli, L. Conti and V. Lubicz, *The $t \to WZ\, b$ decay in the standard model: A Critical reanalysis*, *Phys.Lett.* **B502** (2001) 125–132 [hep-ph/0010090].

[31] R. Decker, M. Nowakowski and A. Pilaftsis, *Dominant three-body decays of a heavy Higgs and top quark*, *Z.Phys.* **C57** (1993) 339–348 [hep-ph/9301283].

[32] G. Mahlon and S. J. Parke, *Finite width effects in top quark decays*, *Phys.Lett.* **B347** (1995) 394–398 [hep-ph/9412250].

[33] E. E. Jenkins, *The Rare top decays $t \to bW^+Z$ and $t \to cW^+W^-$*, *Phys.Rev.* **D56** (1997) 458–466 [hep-ph/9612211].

[34] G. Ossola, C. G. Papadopoulos and R. Pittau, *Reducing full one-loop amplitudes to scalar integrals at the integrand level*, *Nucl.Phys.* **B763** (2007) 147–169 [hep-ph/0609007].

[35] R. K. Ellis, W. Giele and Z. Kunszt, *A Numerical Unitarity Formalism for Evaluating One-Loop Amplitudes*, *JHEP* **0803** (2008) 003 [0708.2398].

[36] W. T. Giele, Z. Kunszt and K. Melnikov, *Full one-loop amplitudes from tree amplitudes*, *JHEP* **0804** (2008) 049 [0801.2237].

[37] R. K. Ellis, W. T. Giele, Z. Kunszt and K. Melnikov, *Masses, fermions and generalized D-dimensional unitarity*, *Nucl.Phys.* **B822** (2009) 270–282 [0806.3467].

[38] R. K. Ellis, Z. Kunszt, K. Melnikov and G. Zanderighi, *One-loop calculations in quantum field theory: from Feynman diagrams to unitarity cuts*, *Phys.Rept.* **518** (2012) 141–250 [1105.4319].

[39] K. Melnikov and M. Schulze, *NLO QCD corrections to top quark pair production and decay at hadron colliders*, *JHEP* **0908** (2009) 049 [0907.3090].

[40] R. K. Ellis, W. Giele, Z. Kunszt, K. Melnikov and G. Zanderighi, *One-loop amplitudes for W^+ 3 jet production in hadron collisions*, *JHEP* **0901** (2009) 012 [0810.2762].

[41] S. Catani and M. Seymour, *A General algorithm for calculating jet cross-sections in NLO QCD*, *Nucl.Phys.* **B485** (1997) 291–419 [hep-ph/9605323].

[42] S. Catani, S. Dittmaier, M. H. Seymour and Z. Trocsanyi, *The Dipole formalism for next-to-leading order QCD calculations with massive partons*, *Nucl.Phys.* **B627** (2002) 189–265 [hep-ph/0201036].

[43] Z. Nagy and Z. Trocsanyi, *Next-to-leading order calculation of four jet observables in electron positron annihilation*, *Phys.Rev.* **D59** (1999) 014020 [hep-ph/9806317].

[44] Z. Nagy, *Next-to-leading order calculation of three jet observables in hadron hadron collision*, *Phys.Rev.* **D68** (2003) 094002 [hep-ph/0307268].

[45] G. Bevilacqua, M. Czakon, C. Papadopoulos, R. Pittau and M. Worek, *Assault on the NLO Wishlist: pp → t anti-t b anti-b*, *JHEP* **0909** (2009) 109 [0907.4723].

[46] J. M. Campbell and R. Ellis, *MCFM for the Tevatron and the LHC*, *Nucl.Phys.Proc.Suppl.* **205-206** (2010) 10–15 [1007.3492].

[47] K. Melnikov, M. Schulze and A. Scharf, *QCD corrections to top quark pair production in association with a photon at hadron colliders*, *Phys.Rev.* **D83** (2011) 074013 [1102.1967].

[48] R. Kreckel, *Parallel version of G.P.Lepage's VEGAS-algorithm*, 2000.

[49] Message Passing Interface Forum, *MPI2: A message passing interface standard*, *High Performance Computing Applications* **12** (1998), no. 1–2 1–299.

[50] T. Stelzer and W. Long, *Automatic generation of tree level helicity amplitudes*, *Comput.Phys.Commun.* **81** (1994) 357–371 [hep-ph/9401258].

[51] G. Cullen, N. Greiner, G. Heinrich, G. Luisoni, P. Mastrolia *et. al.*, *Automated One-Loop Calculations with GoSam*, *Eur.Phys.J.* **C72** (2012) 1889 [1111.2034].

[52] J. Pumplin, D. Stump, J. Huston, H. Lai, P. M. Nadolsky *et. al.*, *New generation of parton distributions with uncertainties from global QCD analysis*, *JHEP* **0207** (2002) 012 [hep-ph/0201195].

[53] P. M. Nadolsky, H.-L. Lai, Q.-H. Cao, J. Huston, J. Pumplin *et. al.*, *Implications of CTEQ global analysis for collider observables*, *Phys.Rev.* **D78** (2008) 013004 [0802.0007].

[54] J. Alcaraz Maestre *et. al.*, *The SM and NLO Multileg and SM MC Working Groups: Summary Report*, 1203.6803.

[55] J. Aguilar-Saavedra, *A Minimal set of top anomalous couplings*, *Nucl.Phys.* **B812** (2009) 181–204 [0811.3842].

[56] C. Zhang, N. Greiner and S. Willenbrock, *Constraints on Non-standard Top Quark Couplings*, *Phys.Rev.* **D86** (2012) 014024 [1201.6670].

[57] J. Bernabeu, D. Comelli, L. Lavoura and J. P. Silva, *Weak magnetic dipole moments in two Higgs doublet models*, *Phys.Rev.* **D53** (1996) 5222–5232 [hep-ph/9509416].

[58] W. Hollik, J. I. Illana, S. Rigolin, C. Schappacher and D. Stockinger, *Top dipole form-factors and loop induced CP violation in supersymmetry*, *Nucl.Phys.* **B551** (1999) 3–40 [hep-ph/9812298].

[59] P. Mastrolia, E. Mirabella and T. Peraro, *Integrand reduction of one-loop scattering amplitudes through Laurent series expansion*, *JHEP* **1206** (2012) 095 [1203.0291].

[60] M. Ciuchini, E. Franco, S. Mishima and L. Silvestrini, *Electroweak Precision Observables, New Physics and the Nature of a 126 GeV Higgs Boson*, *JHEP* **1308** (2013) 106 [1306.4644].

[61] G. Altarelli and R. Barbieri, *Vacuum polarization effects of new physics on electroweak processes*, *Phys.Lett.* **B253** (1991) 161–167.

[62] G. Altarelli, R. Barbieri and S. Jadach, *Toward a model independent analysis of electroweak data*, *Nucl.Phys.* **B369** (1992) 3–32.

[63] G. Altarelli, R. Barbieri and F. Caravaglios, *Nonstandard analysis of electroweak precision data*, *Nucl.Phys.* **B405** (1993) 3–23.

[64] F. Larios, M. Perez and C. Yuan, *Analysis of tbW and ttZ couplings from CLEO and LEP / SLC data*, *Phys.Lett.* **B457** (1999) 334–340 [hep-ph/9903394].

[65] A. Martin, W. Stirling, R. Thorne and G. Watt, *Parton distributions for the LHC*, *Eur.Phys.J.* **C63** (2009) 189–285 [0901.0002].

[66] M. Cacciari, G. P. Salam and G. Soyez, *The Anti-k(t) jet clustering algorithm*, *JHEP* **0804** (2008) 063 [0802.1189].

[67] H.-L. Lai, M. Guzzi, J. Huston, Z. Li, P. M. Nadolsky *et. al.*, *New parton distributions for collider physics*, *Phys.Rev.* **D82** (2010) 074024 [1007.2241].

[68] G. Cowan, K. Cranmer, E. Gross and O. Vitells, *Asymptotic formulae for likelihood-based tests of new physics*, *Eur.Phys.J.* **C71** (2011) 1554 [1007.1727].

[69] G. J. Feldman and R. D. Cousins, *A Unified approach to the classical statistical analysis of small signals*, *Phys.Rev.* **D57** (1998) 3873–3889 [physics/9711021].

[70] J. Conway, *Incorporating Nuisance Parameters in Likelihoods for Multisource Spectra*, 1103.0354.

[71] J. Neyman and E. S. Pearson, *On the Problem of the Most Efficient Tests of Statistical Hypotheses*, *Philosophical Transactions of the Royal Society* **231** (1933) 694–706.

[72] F. del Aguila, M. Perez-Victoria and J. Santiago, *Observable contributions of new exotic quarks to quark mixing*, *JHEP* **0009** (2000) 011 [hep-ph/0007316].